KSME

Springer

Journal of Mechanical Science and Technology 35 (4) 2021

Original Article
DOI 10.1007/s12206-021-0324-7

Keywords:
· Multi-lattice structure
· Strut-based design
· Equivalent elastic properties
· Topology optimization
· Additive manufacturing
· DfAM

Correspondence to:
Sang Hu Park
sanghu@pusan.ac.kr

Citation:
Jeong, H. S., Lyu, S.-K., Park, S. H. (2021). Effective strut-based design approach of multi-shaped lattices using equivalent material properties. Journal of Mechanical Science and Technology 35 (4) (2021) 1609~1622.
http://doi.org/10.1007/s12206-021-0324-7

Received September 24th, 2020
Revised December 22nd, 2020
Accepted December 27th, 2020

† Recommended by Editor Seungjae Min

Effective strut-based design approach of multi-shaped lattices using equivalent material properties

Ho Seung Jeong[1], Sung-Ki Lyu[2] and Sang Hu Park[3]

[1]BK21 Plus, School of Mechanical Engineering, Pusan National University, 2, Busandaehak-ro 63 beon-gil, Geumjeong-gu, Busan 46241, Korea, [2]School of Mechanical and Aerospace Engineering, Gyeongsang National University, 501 Jinju-daero, Jinju 52828, Korea, [3]School of Mechanical Engineering, ERC/NSDM, Pusan National University, 2, Busandaehak-ro 63 beon-gil, Geumjeong-gu, Busan 46241, Korea

Abstract We propose an effective approach for designing a multi-lattice structure (MLS) that simultaneously considers local densities and the fillet-joint shape of struts to express practical equivalent material properties. The density of each cell is optimized by changing the strut diameter and fillet-joint radius according to loading conditions. The equivalent material properties of MLS, such as elastic modulus and shear modulus, are calculated based on a computational homogenization method. Finite element analyses of the full-shape and homogenized lattice model under external compressive load are conducted to evaluate the equivalent material properties. We also designed an optimized three-point bending structure using the proposed method. Based on the results of the topology optimization, three types of lattices with different relative densities are designed in a local zone considering local deformation modes. The result of this work shows that multi-lattice bending structure has about 86.9 % higher strength than that of a uniform BCC lattice structure with the same weight.

1. Introduction

Recently, additive manufacturing (AM), particularly laser-based AM, has been widely used to fabricate three-dimensional (3D) structures via layer-by-layer accumulation from a digital model. The 3D high valuable and complicated structures are generally difficult to fabricate using conventional processes, such as casting, machining, and press-forming [1-4]. However, demand for highly functional parts with lightweight [5] and compactness [6], strength [7], wearproof [8], metamaterials [9], shape-memory [10], cellular composites [11, 12], and productivity to increase energy savings has increased steeply every year. AM technology is also being used to fabricate personalized medical devices for the protection against the spread of diseases and viruses such as COVID19 [13]. As industrial applications, inner lattice structures between plates or on the inside of mechanical parts are widely used to obtain lightweight and high-strength properties [14, 15]. These inner architectures can provide excellent energy absorption characteristics and good thermal and acoustic insulation properties [16, 17]. Sandwich panels [18, 19], vibration and sound insulators [20], compact heat exchangers [21, 22], and biomedical implant areas [23-26] have been reported to be valuable applications of the lattice structure.

Generally, the lattice structures can be classified into two types: surface-based and strut-based lattice structures. A surface-based lattice or inner structure used in a sandwich panel has a millimeter-scale dimension and wavy shape; hence, it can be fabricated easily using a conventional press-bending process. Meanwhile, a strut-based lattice is structured as a network of sub-millimeter scale struts in a 3D space [27]. Therefore, controlling design parameters, such as geometrical shape and size, strut diameter, and base material, are important [28]. A recent study reports that damage-tolerant materials can be developed using strut-based lattices inspired by crystal microstructure [29]. The behavior of lattices can be controlled through the adap-

tive design of the lattice units, realizing unprecedented material properties, such as superlight mass with high strength. However, designing a strut-based lattice is not simple because predicting the mechanical properties of the strut-based lattice requires using computational analysis. In the analysis, complicated modeling and meshing are required to consider the real shape of lattices. However, the equivalent material property of lattices represented as equivalent material modulus and shear modulus can be used instead of the real shape-based property of the lattice structures.

Until recently, some studies on the equivalent mechanical properties, which are obtained using numerical or experiment-based theoretical analyses, are reported to predict the material properties of architectured structures [27, 30-36]. Gibson et al. introduced the scaling law, which describes the mechanical properties of lattice structures as a function of relative density [37]. Deshpande et al. conducted an experimental and theoretical investigation to identify equivalent mechanical properties [30-33]. A homogenization method is also implemented to determine the mechanical behavior of the equivalent homogeneous anisotropic medium at the macroscopic scale [34-36, 38]. The computational homogenization method is efficient in predicting the equivalent material properties of lattice structures. Chen et al. estimated the equivalent mechanical properties of asymmetric honeycomb structures by incorporating shear, bending, and tensile deformation [34]. Kaur et al. conducted a study to enhance the mechanical properties of stretching-dominated and bending-dominated lattice structures fabricated using the AM process [38]. Maskery et al. conducted a numerical analysis to design triply periodic minimal surfaces (TPMS) with gradient-density lattice structures [27].

However, the geometric shape of a lattice unit is an important parameter in the basic design step of DfAM (design for additive manufacturing). Many studies on the efficient shape and optimization of lightweight lattice structures for AM [36, 39-48]. Mahmoud et al. reviewed the application of functionally graded lattice structures to improve or control the mechanical properties of orthopedic implants [25]. Panesar et al. proposed uniform, intersected, graded, and scaled lattice design strategies in terms of structural strength and AM-related manufacturing considerations. The lattice structures derived from the topology optimization are found to be superior to uniform lattice structures [39]. Alzahrani et al. proposed a design method for lightweight truss-like lattice structures that considers their relative density obtained from solid topology optimization [40]. Cheng et al. presented a homogenization-based topology optimization (HMTO) method to optimize the design of a lattice structure to achieve lightweight design efficiently [41-47]. Daynes et al. designed and optimized lattice structures based on the isostatic line aligned with principle stresses [48]. They conducted a three-point bending test using a single shape specimen with different lattice diameters to validate their proposed method. Although drastic progress has been made in lattice research in terms of design, manufacturing, and application, most studies were conducted based on a single lattice with equal strut diameter. Furthermore, exact modeling of lattices to predict mechanical behaviors is time-consuming and effortful because of the intricate shapes and orientations.

In this study, using homogenized topology optimization with considering a real shape of strut-like fillet-joints, we focused on an effective and simple design method to reduce the effort required in direct modeling multi-lattices. For the optimization of the lightweight and highly stiff structure, three types of strut-based lattices, namely, simple cubic (SC), body-centered cubic (BCC), and octahedral cubic (OTC), which are frequently used as inner lattice structures in previous studies [46], are first introduced considering real shapes of lattices, such as with and without edge fillet radius. A correlation between strut diameter and relative density of unit lattice is obtained to determine the geometric dimensions of the lattice structure in terms of relative density. Further, for efficient computational simulation, the equivalent material properties of a lattice obtained from a homogenization method are used in the analysis. The usefulness of this approach is evaluated by comparing the analysis results of a full-shaped model with those of a simplified effective model. Using the proposed approach, a three-point bending specimen is optimized to obtain a higher stiffness-to-weight ratio.

2. Design process based on homogenization of strut-based lattice

Generally, strut-based lattices have a complex 3D truss-like structure with interconnected struts and nodes. In finite element (FE) analysis, the shape and element size affects the accuracy of the analysis results. Particularly, the accuracy of the analysis results for complex lattice structures corresponds to the element size [31]. A high-performance computer system and long computation time are commonly required to evaluate the exact mechanical properties of complex lattice structures using computational simulation. Therefore, equivalent elastic properties corresponding to complex lattice structures for efficient computational simulation is essentially required. Recently, several studies investigated the equivalent elastic properties of various lattice structures. Most studies investigated the lattice geometry without edge fillets at the strut intersections. Further, the failure of the strut-based lattice is observed to occur at the strut intersections [46, 49].

This study employed three types of strut-based lattice structure: SC_R, BCC_R, and OTC_R with small edge fillet designed or formed naturally in the AM process ($r^* = r_L / l_L$ = 0.04). Here, r^* is the relative edge fillet, r_L is the radius of edge fillet in lattice unit cell, and l_L is the length of one side of the lattice unit cell. The subscript R represents the lattice structure with edge fillets. Fig. 1 shows the three types of strut-based lattice structures used in this work. Stretch-dominated lattices, such as OTC, are used for relatively high stiffness and strength, while bend-dominated structures, such as stochastic foam and BCC, are relatively widely used for energy absorption [16, 30, 38, 50, 53].

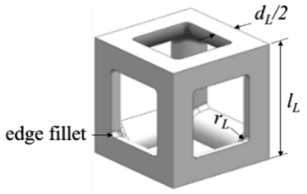

(a) SC_R (d^* = 0.410)

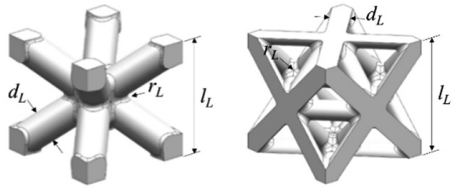

(b) BCC_R (d^* = 0.268) (c) OTC_R (d^* = 0.169)

Fig. 1. Three types of strut-based lattice structure with small edge fillet (ρ^* = 0.3).

2.1 Calculation of relative strut diameter

The relationship between the relative density and detailed dimensions of the lattice geometry should be defined to estimate a design parameter of lattice structures in terms of the relative density. The strut diameter of the lattice is dependent on the relative density ($d^* = d_L / l_L$) of the lattice structure, and can be expressed in terms of the relative density ($\rho^* = \rho_L / \rho_S$), where d_L is the strut diameter in a lattice unit cell, ρ_L is the density of a lattice unit cell, and ρ_s is the density of a solid unit cell [36-39]. Regression equations of the second to fifth-order are evaluated to determine the best regression equation for the lattice density and relative strut diameter between 0 to 1 obtained from the CAD model. Fig. 2(a) shows the raw data of OTC_R and the curve of the second to the fifth-order regression equation, and Fig. 2(b) shows the ratios of the raw data and higher-order equations. It is calculated that the maximum difference between the fifth-order regression equation and the raw data is within about 0.2 %, and the maximum difference between the third-order regression equation and the raw data is increased by about 4 %. Thus, we know that the higher-order regression equation is more accurate than the lower order.

The relationship for the relative strut diameter in terms of the relative density is obtained for the six types of lattice structures with and without edge fillet radius. Fig. 2(c) and Table 1 show that the relationship between the relative strut diameter with and without edge fillets and the relative density is expressed as a fifth-order regression equation for an accurate fit. Table 1 lists the coefficients of the regression equation to calculate the relative strut diameter. The regression equation is expressed as Eq. (1), which is meaningful in the range of relative density from 0.2 to 0.8.

$$d^* = f(\rho^*) = a_0 + a_1(\rho^*) + a_2(\rho^*)^2 + a_3(\rho^*)^3 + a_4(\rho^*)^4 + a_5(\rho^*)^5 \quad (1)$$

Table 1. Coefficients of regression equations for the relative strut diameter (d*) according to the relative density.

Relative strut diameter	a_0	a_1	a_2	a_3	a_4	a_5
d^*_{BCC}	0.0467	1.1904	-2.5906	4.9331	-4.7789	1.8956
$d^*_{BCC_R}$	0.0455	1.1969	-2.6153	4.9178	-4.6882	1.8317
d^*_{SC}	0.0809	1.6616	-3.1607	5.7628	-5.5309	2.2683
$d^*_{SC_R}$	0.0799	1.6678	-3.2162	5.9326	-5.7438	2.3587
d^*_{OTC}	0.0331	0.7248	-1.5199	3.0306	-3.1598	1.3750
$d^*_{OTC_R}$	0.0287	0.7312	-1.5453	3.0022	-3.0134	1.2528

The relative strut diameters of the lattice structures are compared at a relative density of 0.3. The relative strut diameters of the SC_R, BCC_R, and OTC_R structures are 0.41, 0.268, and 0.169, respectively. The SC_R strut diameter of 0.41 is 2.43 times larger than that of the OTC_R of 0.169. Further, the relative strut diameters of the lattice structures with and without edge fillets are compared. At a relative density of 0.3, the relative strut diameters of the SC_R, BCC_R, and OTC_R lattice structures with edge fillet decreased by 0.26, 0.49, and 2.75 %, respectively, when compared with those of the models without edge fillet.

2.2 Equivalent elastic properties of lattice

For a density-based lightweight design, the mechanical properties of the lattice structure are required in terms of the relative density. According to the Gibson-Ashby model, the elastic modulus E and shear modulus G of lattice structures are functions of the relative density. These functions are called “scaling laws” [22, 24, 30]. Homogenization methods are often used to obtain the equivalent mechanical properties of periodic lattice structures. The lattice structures are generally anisotropic rather than isotropic [26]. The anisotropic constitutive law, $\{\sigma\} = [C]\{\varepsilon\}$, is used for the mechanical properties of the lattice structure, where $\{\sigma\}$, $[C]$, and $\{\varepsilon\}$ are the stress, stiffness matrix, and strains respectively. To obtain the equivalent stiffness matrix, Established periodic boundary conditions (PBCs) are applied to the unit cell of a lattice structure to obtain the equivalent stiffness matrix. At each time, the PBCs are applied, such that one strain component in one-direction is set to unity and the other strains are set to zero. The stiffness matrix $[C]$ of a unit cell is calculated using the FE simulation. The elastic modulus, shear modulus, and Poisson’s ratio are driven by the compliance matrix $[S]$ obtained by inverting the stiffness matrix $[C]$ as following Eq. (2) [31]:

$$[S] = [C]^{-1}$$
$$E_1 = \frac{1}{S_{11}},\ \upsilon_{12} = -\frac{S_{12}}{S_{11}},\ G_{12} = \frac{1}{S_{66}}$$

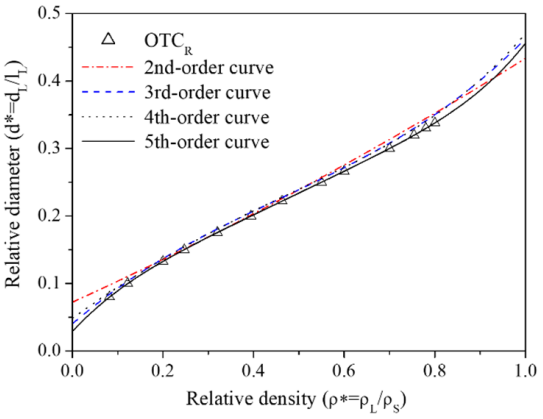

(a) Second-order to fifth-order regression equation for OTC$_R$

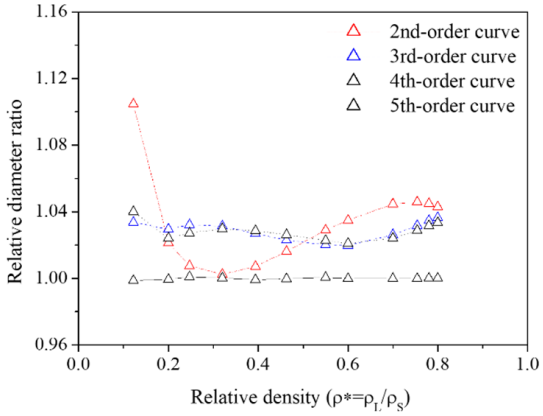

(b) Ratios of the raw data and higher-order regression equations for OTC$_R$

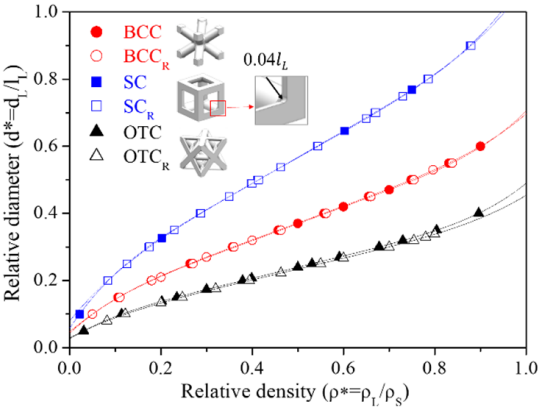

(c) Fifth-order regression equations for the six types of lattice structures

Fig. 2. Relationship between the relative strut diameter and the relative density.

$$E_2=\frac{1}{S_{22}},\ \upsilon_{13}=-\frac{S_{13}}{S_{11}},\ G_{13}=\frac{1}{S_{55}} \qquad (2)$$
$$E_3=\frac{1}{S_{33}},\ \upsilon_{23}=-\frac{S_{23}}{S_{22}},\ G_{23}=\frac{1}{S_{44}}$$

where E_i is the elastic modulus of the material in direction i, G_{ij} is the shear modulus that representing the shear stiffness in the corresponding plane and υ_{ij} is the Poisson's ratio representing the ratio of a transverse strain to the applied strain.

In this study, the equivalent elastic properties for the lattice structure with and without edge fillets at the strut intersections are calculated using the computational homogenization method. The elastic modulus and shear modulus are obtained by applying a uniaxial tension loading and pure shear loading, respectively. For the uniaxial tension loading in the X-direction, the boundary conditions applied are as follows (Eq. (3)) :

$$U_{DCGH}-U_{ABFE}=l,\ V_{ADHE}-V_{BCGF}=0,\ W_{EFGH}-W_{ABCD}=0. \qquad (3)$$

For the pure shear loading in the X-Y plane, the boundary conditions applied are as follows (Eq. (4)):

$$\begin{aligned} &U_{DCGH}-U_{ABFE}=0,\quad V_{DCGH}-V_{ABFE}=l/2\\ &U_{ADHE}-U_{BCGF}=l/2,\ V_{ADHE}-V_{BCGF}=0\\ &W_{ABCD}-W_{EFGH}=0 \end{aligned} \qquad (4)$$

where l is the length of unit lattice cell, $U_{\alpha\beta\gamma\delta}$, $V_{\alpha\beta\gamma\delta}$, and $W_{\alpha\beta\gamma\delta}$ are the displacement components along X, Y, and Z, respectively, and the suffix codes α, β, γ, and δ are the positions of the vertices.

Fig. 3 shows the FE model, uniaxial and pure shear deformation geometries, and boundary conditions for the OTC$_R$ structures. The length of the unit lattice cell used is 1 mm, the diameter of the strut is 0.1 mm, the fillet radius is 0.04 mm, and the relative density condition is 0.1225. A 3-D ten-node tetrahedral structural solid element was used to generate a finite element model. The number of elements and nodes used is 451164 and 665438, respectively. ANSYS software (ver. 2020R1) is used for FE simulation and mesh generation.

The equivalent elastic properties of the lattice unit cell corresponding to various relative densities are obtained. Fig. 4 shows the relative elastic modulus ($E^*=E_L/E_S$) and relative shear modulus ($G^*=G_L/G_S$) in terms of the relative density. Here, E_L and G_L are the elastic modulus and shear modulus in a lattice unit cell, respectively. The third- and fourth-order regression equations are evaluated to obtain an accurate regression equation for the lattice density and relative elastic and shear modulus. In the case of the fourth-order equation, the maximum difference is less than 0.2 % for OCT$_R$. The relationship for the relative elastic and shear modulus in terms of the relative density is obtained for the six types of lattice structures as defined in Figs. 4(a) and (b), respectively. Tables 2 and 3 summarize the coefficients of regression equations for the relatively elastic and shear modulus in terms of the relative density, respectively. The relationship between the equivalent elastic properties and relative density is expressed by the fourth-order regression equation as shown in Eq. (5).

$$E^*=G^*=f\left(\rho^*\right)=a_0+a_1\left(\rho^*\right)+a_2\left(\rho^*\right)^2+a_3\left(\rho^*\right)^3+a_4\left(\rho^*\right)^4. \qquad (5)$$

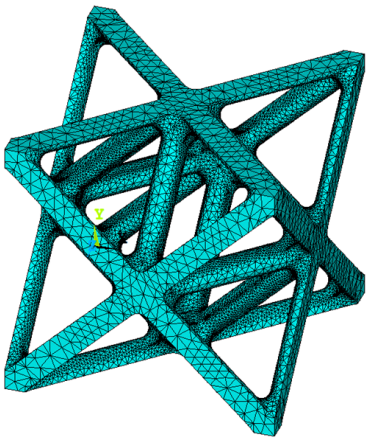

(a) FE model

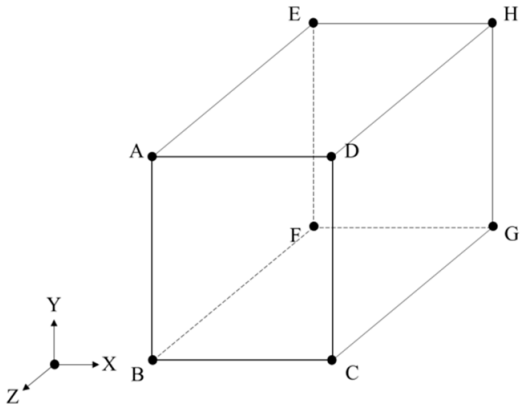

(b) Prescribed PBC of the 3-D model

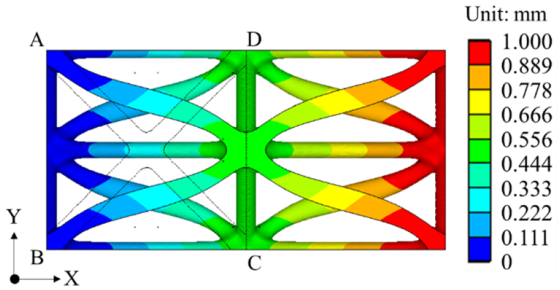

(c) Uniaxial deformation

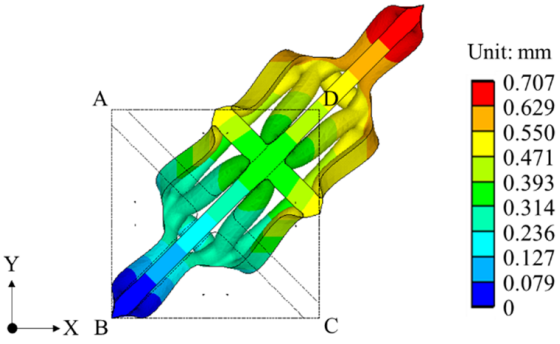

(d) Pure shear deformation

Fig. 3. FE model, PBC and uniaxial and pure shear deformation geometries of OTC_R lattice structures (ρ^* = 0.1225).

Table 2. Coefficients of regression equations for the relative elastic modulus according to the relative density.

Relative strut diameter	a_0	a_1	a_2	a_3	a_4
E^*_{BCC}	0.0017	-0.0197	0.1825	0.4814	0.4572
$E^*_{BCC_R}$	-0.0149	0.1943	-0.7452	2.4034	-0.7913
E^*_{SC}	0.0072	0.2864	0.7606	-0.6371	0.6101
$E^*_{SC_R}$	-0.0019	0.3993	0.3437	0.0583	0.2011
E^*_{OTC}	0.0066	0.0177	0.8442	-1.0472	1.3016
$E^*_{OTC_R}$	-0.0009	0.1314	0.327	0.0959	0.5627

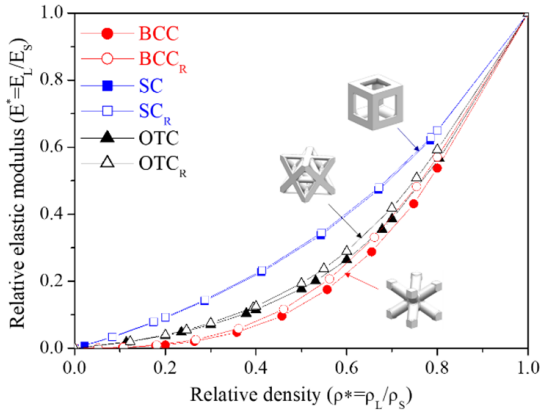

(a) Relative elastic modulus

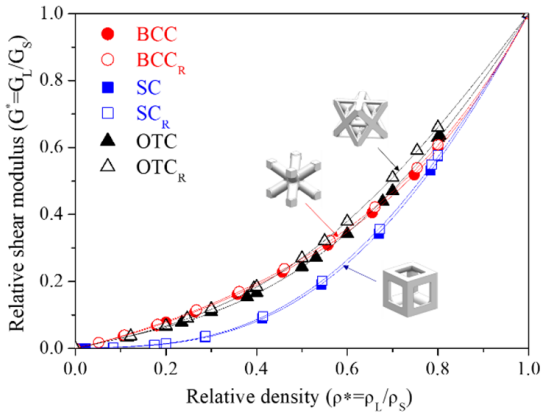

(b) Relative shear modulus

Fig. 4. Relationship for the relative elastic and shear modulus in terms of the relative density.

The relative elastic and shear modulus of the lattice structures with and without edge fillets are compared, as shown in Figs. 5(a) and (b), respectively. At a relative density of 0.4, the elastic modulus and shear modulus of the SC_R, BCC_R, and OTC_R lattice structures with edge fillet increased by 1.6 %, 17.8 %, and 8.6 % and 5.8 %, 3.1 %, and 11.7 %, respectively, when compared with those of the models without edge fillet. In addition, the small edge fillet (r* = 0.04) of a lattice structure

Table 3. Coefficients of regression equations for the relative shear modulus according to the relative density.

Relative strut diameter	a_0	a_1	a_2	a_3	a_4
G^*_{BCC}	0.0044	0.2390	0.7805	-0.9318	0.9274
$G^*_{BCC_R}$	0.0026	0.2789	0.6457	-0.6486	0.7353
G^*_{SC}	0.0033	-0.0571	0.4486	0.3325	0.3778
$G^*_{SC_R}$	-0.0005	0.0124	0.0990	1.1172	-0.1665
G^*_{OTC}	-0.0065	0.3365	-0.1034	0.8764	-0.0390
$G^*_{OTC_R}$	-0.0147	0.4657	-0.6720	2.3056	-1.0929

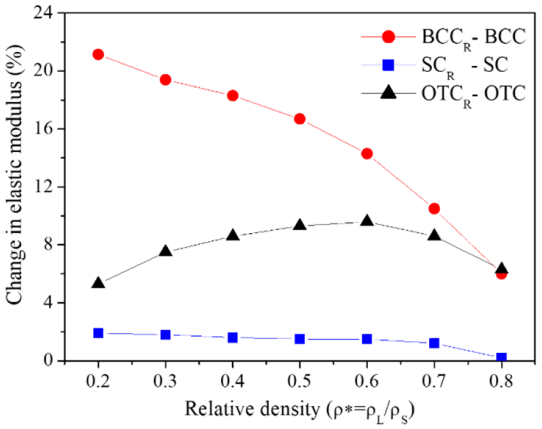

(a) Change in elastic modulus

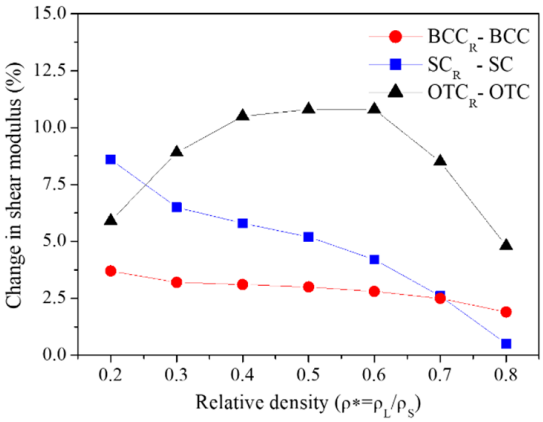

(b) Change in shear modulus

Fig. 5. Comparison of relative elastic and shear modulus of the lattice structures with and without edge fillets.

contributes to increased equivalent elastic properties under an equal-weight condition.

2.3 Evaluation of equivalent elastic properties

Compression simulations are performed on the full-shape and homogenized lattice structure models to validate the predicted equivalent elastic properties. Fig. 6 shows a CAD model of the fourth OTC_R full-shape and a FE model of the fourth OTC_R full-shape and homogenized lattice structure with an edge fillet used in the compression simulation. The number of elements used in the 1/4 full-shape model is approximately 864078. In contrast, the number of elements used in the 1/4 homogenized model is 576. The compression simulation model consists of six layers of lattice structure having a height of 6.5 l_L under a relative density condition of 0.463 in the core, and a 0.25 l_L mm plate on the top and bottom where l_L (= 5 mm) is the length of unit lattice cell. The basic dimensions of the compression model are 30×30×32.5 mm^3. The full-shape model requires a long simulation time because of its numerous elements; hence, the one-fourth full-shape model is used. The displacement constraints are applied to be fixed in the vertical

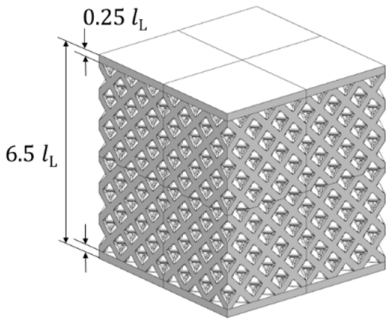

(a) Full-shape CAD model (OTC_R)

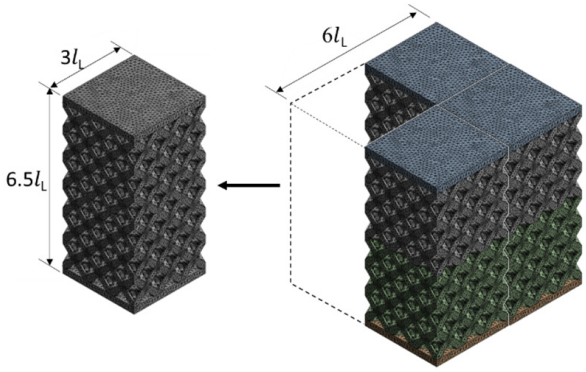

(b) 1/4 full-shape FE model (OTC_R)

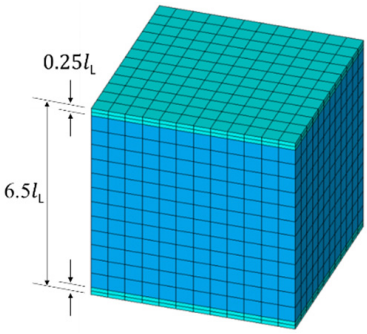

(c) Homogenized FE model

Fig. 6. Full-shape CAD model and 1/4 OTC_R full-shape and homogenized lattice structure FE model used in the compression simulation.

Table 4. Summary of initial stiffness obtained from the compression simulation.

Lattice type		Homogenized model (A)			Full-shape model (B)			Stiffness ratio of homogenized model/full-shape model (A/B)
		Max. disp. (mm)	Initial stiffness (N/mm)	Stiffness ratio (D/C)	Max. disp. (mm)	Initial stiffness (N/mm)	Stiffness ratio (D/C)	
BCC	(C)	4.55E-02	6592	1.156	4.67E-02	6428	1.15	1.026
BCC_R	(D)	3.94E-02	7618		4.06E-02	7388		1.031
SC	(C)	1.89E-02	15834	1.015	1.93E-02	15547	1.014	1.018
SC_R	(D)	1.87E-02	16075		1.90E-02	15769		1.019
OTC	(C)	3.17E-02	9449	1.088	3.19E-02	9393	1.085	1.006
OTC_R	(D)	2.92E-02	10285		2.94E-02	10194		1.009

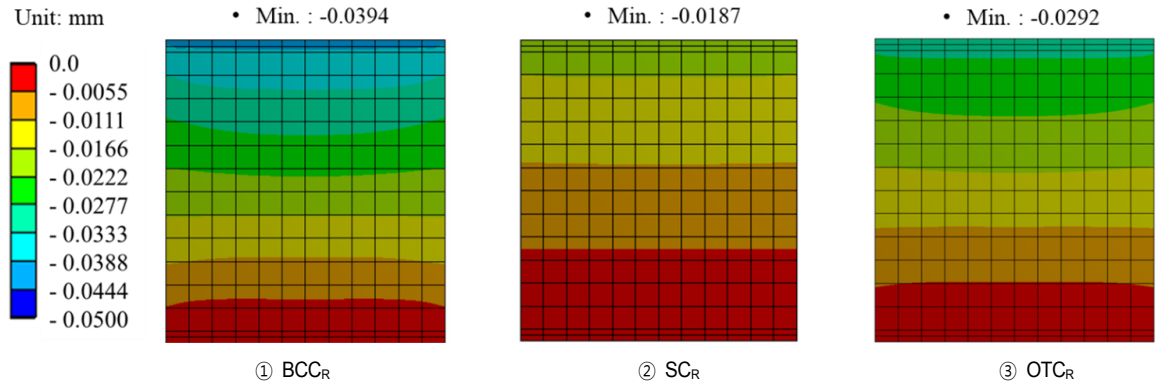

(a) Homogenized model

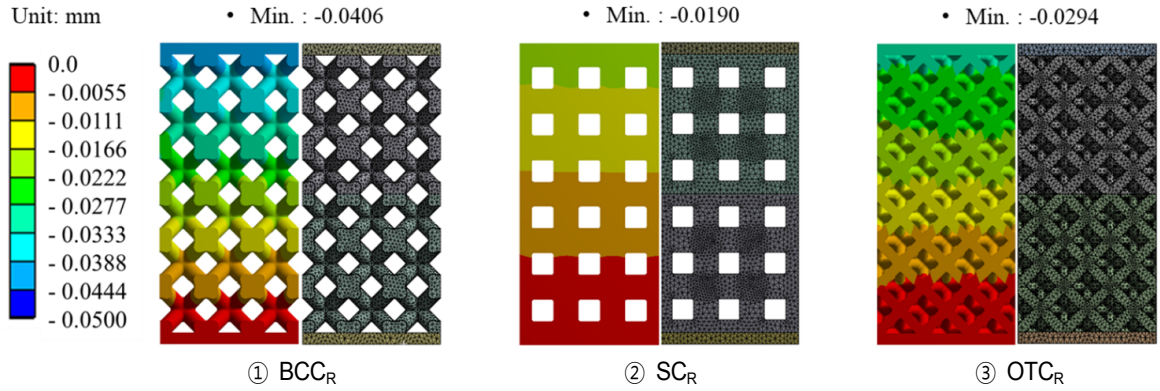

(b) 1/4 full-shape FE model

Fig. 7. Displacement distribution of homogenized model and 1/4 full-shape FE model obtained from the compression simulation.

direction and sliding in the horizontal direction at the supports located on the bottom face of the compression model. Symmetric boundary conditions are applied to the symmetry plane of the compression model, and the 3D 20-node structural solid element is used. A vertical force of 300 N is applied on the top face of the compression model. The material properties are given as a general polymer material. Tensile modules for materials commonly used for stereo lithography apparatus-based 3D printing procured by 3D systems are around 1.6 to 3.4 GPa, and tensile modules for materials used for fused deposition modeling-based 3D printing procured by Stratasys are around 1.7 to 2.2 GPa [44, 45]. Therefore, an elastic modulus of 2 GPa and a Poisson's ratio of 0.3 is given in the compression simulation.

Fig. 7 shows the displacement distribution obtained from the compression simulation. As shown in Table 4, the initial stiffness obtained from the compression simulation results of the full-shape lattice structure model and the homogenized model are compared. This comparison demonstrated an initial stiffness difference of 1 to 3 %. It is confirmed that the equivalent elastic properties predicted by the homogenization method are in good agreement. The uniaxial compression simulation showed that the SC_R lattice structure had relatively high initial stiffness. A close relationship between the directions of the

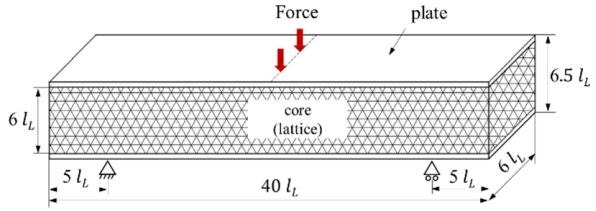

Fig. 8. Basic dimensions and displacement constraints of a sandwich panel.

load and strut was also observed.

3. Application to bending problem

3.1 Topology optimization

In designing a lattice structure with high stiffness and lightweight, a lattice core-based sandwich panel is employed. Conventional sandwich panels consist of a strong outer face and lightweight inner core [18, 19]. Here, density distribution is an important design variable in the optimal design of lattice core structures. Topology optimization is used to obtain a variable density distribution in a lattice core structure. The objective of the topology optimization is to minimize structural compliance. A volume fraction of 40 % is used as a constraint condition, and the minimum relative density (ρ_{min}) and maximum relative density (ρ_{max}) of 0.2 and 0.8, respectively, is applied. Hence, the mathematical expression of the minimum compliance issue for the lattice structure becomes (see Eqs. (6)-(9)):

$$\text{Objective:}\quad f(\rho,U)=U^T K U \tag{6}$$

$$\text{Subjective:}\quad K(\rho)U=F(\rho) \tag{7}$$

$$V^*=\sum_{i=1}^{n} v_i \rho^* \tag{8}$$

$$0.2\le\rho_{min}\le\rho^*\le\rho_{max}\le 0.8 \tag{9}$$

where structural compliance f is the objective function, K is the global stiffness matrix, F is the external load vector, and U is the displacement vector. The first constraint is the equilibrium equation. The second constraint is the elastic scaling law. The third constraint limits the total design volume to V^*. The final constraint requires that the relative density be bounded by the minimum and maximum relative densities. Fig. 8 shows the basic dimensions and displacement constraints of a sandwich panel. The basic dimensions of the sandwich panel are 200 (W)×30 (L)×32.5 (H) mm^3. The displacement constraints are applied to be fixed in the vertical direction and sliding in the horizontal direction at the supports located on the bottom face of the sandwich panel. Symmetry conditions are applied to the middle plane of the sandwich panel in the width and horizontal direction, respectively. A vertical force of 3200 N is applied to the middle of the top face of the sandwich panel.

Fig. 9(a) shows the finite element mesh of a sandwich panel used for topology optimization. The 3D 20-node structural solid element is used. The core of the sandwich panel is defined as the design domain, and the top and bottom plate domains of the sandwich panel is defined as the non-design domain. In addition, to prevent local failure due to concentrated load, the local region of the inner core in contact with the support and load face is defined as the non-designed domain. Further, the equivalent elastic properties obtained from the scaling law of the lattice structures are used for topology optimization. Fig. 9(b) shows the relative density distribution of the lattice at the core in a quarter symmetrical sandwich panel for the three types of lattice obtained from the topology optimization results. It is observed that the density distribution changes according to the type of the lattice structure.

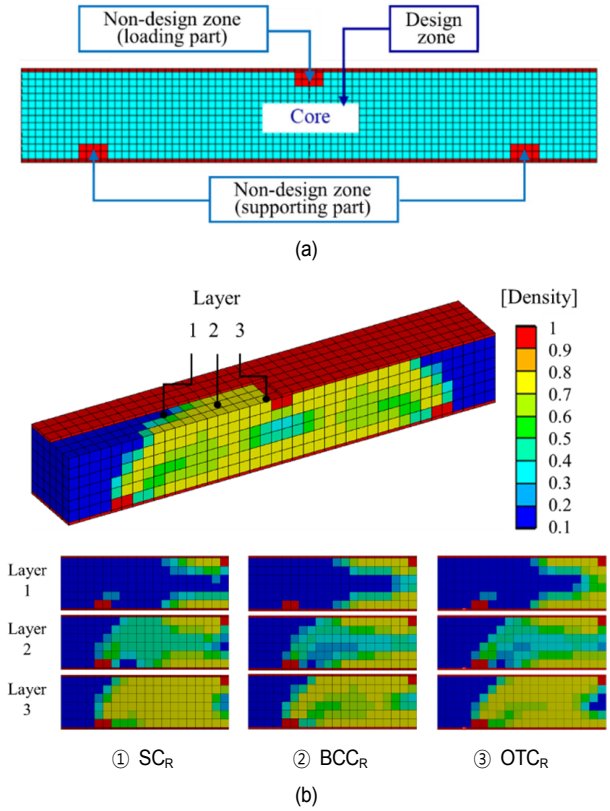

Fig. 9. (a) FE model of a sandwich panel for topology optimization; (b) relative density distribution of lattice structure in the core of the sandwich panel from the topology optimization.

3.2 Multi-lattices structure with diverse local densities

The lattice structure models are constructed with various lattice types, lattice combinations, and relative density distributions. The three types of proposed lattice models are as follows. The first type is a single-density and single-lattice structure model. Four models with a single lattice and uniform relative density of 46.3 % are proposed. The second type is a variable-density and single-lattice structural model with three models with a single lattice and variable density are proposed. The

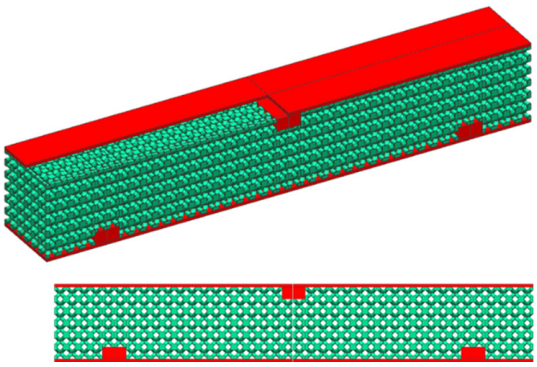

(a) Single-density and single-lattice structure model consist of BCC_R, baseline model (model-2)

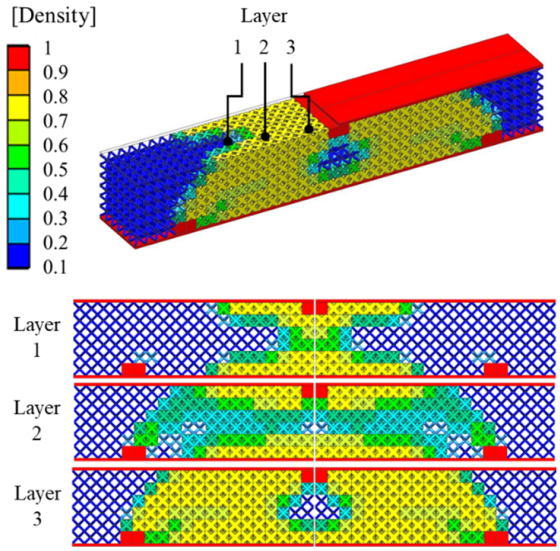

(b) Variable-density and multi-lattice model (frame region: OTC_R, assisted region: BCC_R, model-12)

Fig. 10. 1/4 full-shape model and layer cross-sections of lattice core-based sandwich panel.

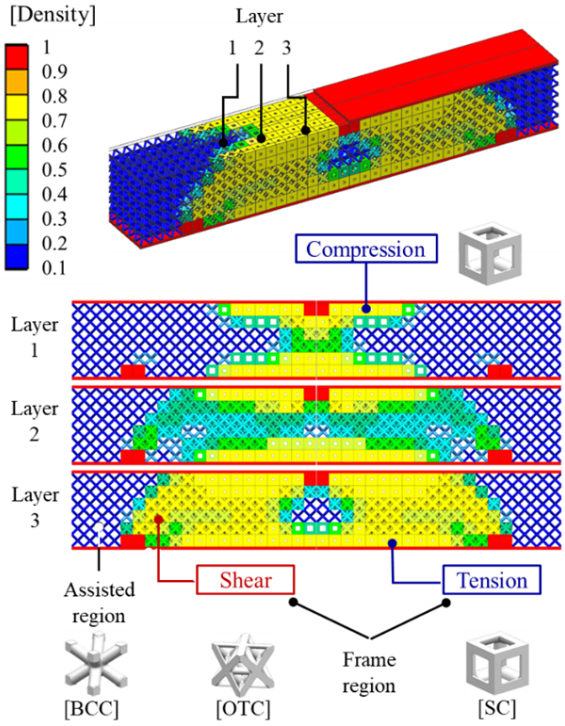

Fig. 11. Variable-density and multi-lattice full-shape model considering the direction of elastic properties of the lattice structure (frame region: OTC_R and SC_R, assisted region: BCC_R, model-14).

third type is a variable-density and multi-lattice structure model. Before constructing a multi-lattice model, the lattice structure model is divided into a frame region and an assisted region. The frame region has a relative density greater than 0.3, while the assisted region has a relative density less than or equal to 0.3. The lattice in the assisted region is self-supporting and fills the entire design domain to maintain the overall structure shape. Here, six models with the different single-lattice structure in the assisted and frame regions, and variable density are proposed. In addition, a model considering the direction of the elastic properties of the lattice structure is proposed. Based on the model consisting of an OTC_R lattice structure (model-12) in the frame region, an additional lattice model (model-14) is constructed by rearranging into SC_R lattice structures with relatively high elastic modulus in regions of the high relative density of 0.8 with the vertical or horizontal distribution. Fig. 10(a) shows a single-density and single-lattice structure model (model-2) consisting of a BCC_R lattice with a small edge fillet and 46.3 % relative density. Fig. 10(b) shows the variable-density and multi-lattice structure model (model-12) consisting of an OTC_R lattice in the frame region and a BCC_R lattice in the assisted region.

Fig. 11 shows the variable-density and multi-lattice structure model considering the direction of elastic properties of the lattice structure (model-14). It consists of an OTC_R and an SC_R lattice in the frame region and a BCC_R lattice in the assisted region.

3.3 Simulation of homogenized and full-shape model

A three-point bending simulation is performed using a homogenized lattice structure model to evaluate the bending stiffness of sandwich panels with various lattice core structures. The homogenized lattice structure model is constructed by considering the equivalent elastic properties of lattice structure corresponding to the relative density distribution obtained from the topology optimization. The bending simulation model used 46.3 % relative density in the core and 51.1 % relative density in the lattice core-based sandwich panel. Material properties at a relative density of 1.0 are used for Young's modulus of 2 GPa and Poisson's ratio of 0.3. Two full-shape simulations are conducted on the three-point bending of lattice structure core-based sandwich panel to validate the design method for the homogenized lattice structure model. A variable-density and multi-lattice structure model is constructed by considering

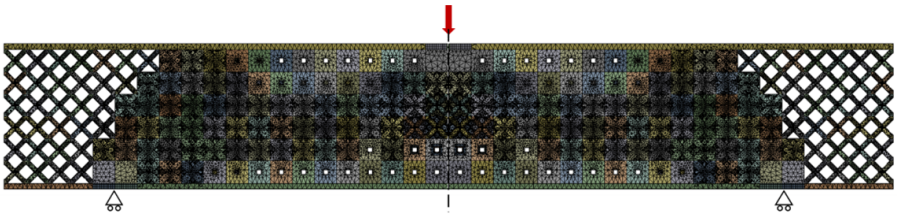

Fig. 12. FE model of a variable-density and multi-lattice core-based full-shape sandwich panel for 3-point bending simulation (model-14).

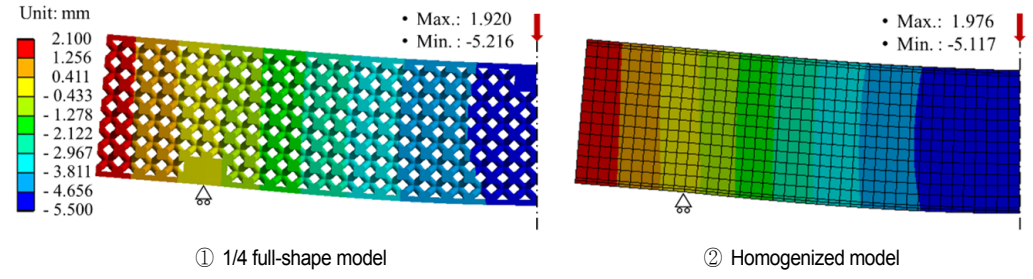

① 1/4 full-shape model ② Homogenized model

(a) Uniform-density and single-lattice model (model-2)

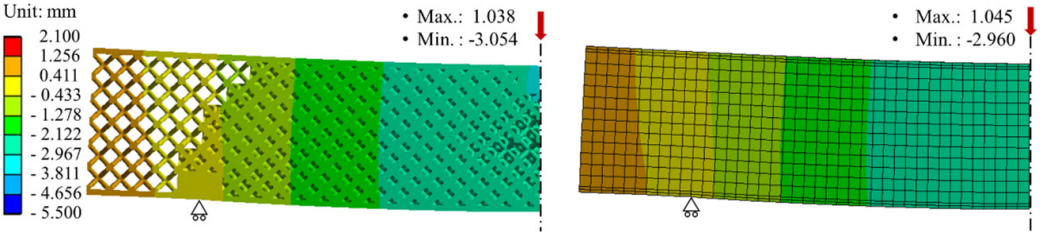

① 1/4 full-shape model ② Homogenized model

(b) Variable-density and multi-lattice model (2 types of lattice, model-12)

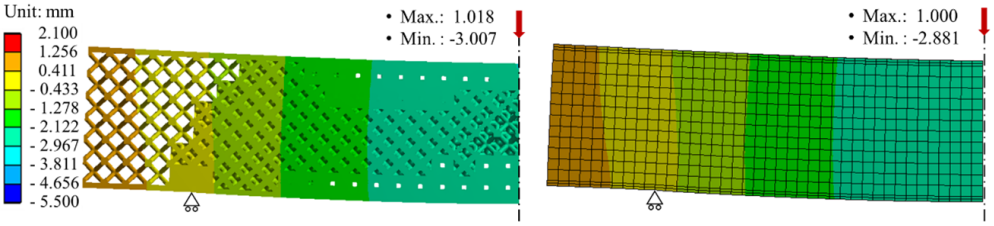

① 1/4 full-shape model ② Homogenized model

(c) Variable-density and multi-lattice model (3 types of lattice, model-14)

Fig. 13. Displacement distribution of variable-density and multi-lattice 1/4 full-shape model.

the geometry of the lattice unit cell corresponding to the relative density distribution. Fig. 12 shows the FE model of the variable-density and multi-lattice full-shape model with an edge fillet used in the three-point bending simulation (model-14). The number of elements of the 1/4 full-shape models is 3058795. In contrast, the number of elements of the 1/4 homogenized model is 3840.

Fig. 13 shows the displacement distribution of the variable-density and multi-lattice 1/4 full-shape model.

Table 5 shows the initial stiffness obtained from the three-point bending simulation results for the full-shape lattice structure model and homogenized model are compared. As a result, an initial stiffness difference of 1 to 4.3 % is observed. Thus, the equivalent elastic properties predicted by the homogenization method are confirmed to be in good agreement.

4. Results and discussion

Compression simulations for 3(W)x3(L)x6(H) lattice structures are performed on the 1/4 full-shape and homogenized lattice structure models to validate the predicted equivalent elastic properties. As a result, an initial stiffness difference of up to 3 % is observed. A three-point bending simulation for the sandwich panel with variable-density and multi-lattice structures are performed on the 1/4 full-shape and homogenized lattice structure models. As a result, an initial stiffness differ-

Table 5. Comparison of simulation and experiment on initial bending stiffness from three-point bending.

Model no.	Lattice type		Simulation				Initial stiffness ratio of homogenized model/full-shape model (B/A)
	Frame region	Assisted region	Homogenized model (B)		Full-shape model (A)		
			Max. deflection, δ (mm)	Initial stiffness, F/δ (N/mm)	Max. deflection, δ (mm)	Initial stiffness, F/δ (N/mm)	
1	BCC	BCC	5.381	0.995	5.362	597	0.995
2	BCC_R	BCC_R	5.117	1.019	5.216	627	1.019
12	OTC_R	BCC_R	2.960	1.032	3.054	1048	1.032
14	OTC_R, SC_R	BCC_R	2.881	1.043	3.007	1064	1.043

ence of up to 4.3 % is observed.

The three-point bending test and full-shaped model simulation results presented in the literature (Cheng et al. 2017) [34] are introduced for validation of the homogenized results. The three-point bending beam model consists of a uniform cubic structure with a relative density of 0.5, specimen size of 120×15×15 mm^3, and unit lattice constant of 2.5 mm. The support position on the bottom surface is located at 9 mm from both ends. Specimens of each uniform beam are printed in VeroWhite. Here, an elastic modulus of 2100 MPa and a Poisson's ratio of 0.3 are used as the mechanical properties of VeroWhite. The equivalent elastic properties of SC (cubic) lattice corresponding to 0.5 relative density are used with an elastic modulus of 627.99 MPa, shear modulus of 99.98 MPa, and Poisson's ratio of 0.16. The three-point bending simulation for the homogenized model is performed. The applied force is 200 N.

Fig. 14 shows the displacement distribution of the homogenized model with a displacement of 1.88 mm. The calculated stiffness is 106.02 N/mm. Table 6 shows that the initial stiffness obtained from the three-point bending results for the homogenized model, full-shaped model simulation, and experiment is compared. The difference in stiffness of full-shaped model simulation, and experiment in literature are 2.3 %, and 9.1 %, respectively. The equivalent elastic properties predicted by the homogenization method are confirmed to be in good agreement with the results reported in the literature. Thus, the predicted stiffness of the homogenized model is approximately equal to that of the homogenized model and full-shaped model simulation reported in the literature.

Comparing the results of the homogenized lattice structure and full-shape models, an initial stiffness difference of 0.5 %-4.3 % is observed. It is confirmed that the mechanical properties predicted by the homogenization method are in good agreement. Thus, the proposed homogenization method and equivalent elastic properties for lattice structures are validated.

The number of elements for the full-shape model and the homogenized model used in the simulation were compared to observe the design efficiency for the lattice structure model. In the compression simulation for a 3(W)x3(L)x6(H) lattice structure, the number of elements used in the full model and the homogenized model is 864078 and 576, respectively. In the three-point bend simulation for a sandwich panel with a

Table 6. Comparison of simulation and experiment on initial bending stiffness from three-point bending [34].

Model type	Simulation		
	Full-shaped model [34]	Experiment [34]	Homogenized model
Uniform beam (N/mm)	108.46	96.34	106.02

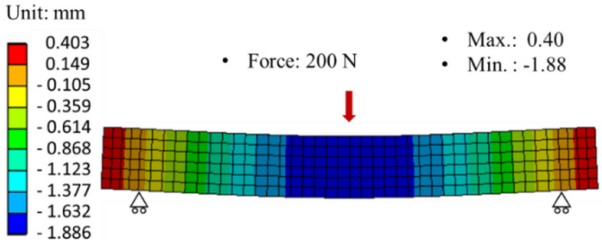

Fig. 14. Displacement distribution of homogenized uniform SC (cubic) lattice model.

3(W)x20(L)x6(H) lattice structure, the number of elements used in the full-shape model and the homogenized model are 3058795 and 3840, respectively. It was confirmed that the homogenized model had relatively few elements used than the full-shape model. The reduction in the number of elements means the computation time in the simulation is reduced dramatically. In addition, the homogenized model was able to reduce 3D CAD modeling time significantly by simplifying the complex lattice structure to a simple cube structure.

In this study, the equivalent elastic properties for the lattice structure with and without edge fillets at the intersections of struts are calculated using the computational homogenization method. The relationship between the equivalent elastic properties and relative density is expressed by the fourth-order regression equation. The equivalent elastic properties of the lattice structures with and without edge fillets are compared. The small edge fillet of lattice structure contributes to increased equivalent elastic properties and improved anisotropy of the lattice under equal-weight conditions.

Kang et al. proposed an optimization method for obtaining lightweight, high strength, and high stiffness of a lattice-based sandwich panel using topology optimization and multi-lattice structures [46]. In the proposed optimization design, the variable

density and multi-lattice core model suggested a 66 % increase in stiffness than that of the single BCC uniform-density lattice core. Table 5 shows the summary of the initial bending stiffness of a homogenized lattice model obtained from the three-point bending simulation. The variable-density and multi-lattice based sandwich panel consisting of three types of lattices (model-14) is found to exhibit approximately 86.9 % higher initial stiffness than those of the conventional BCC uniform density baseline model (model-1). The variable-density and multi-lattice-based sandwich panel consisting of two types of lattices (model-12) is found to exhibit approximately 81.9 % higher initial stiffness than those of the baseline model (model-1).

However, from a manufacturability point of view, the recommended design for the strut diameter should be 0.3 mm or more in the metal AM process [46].

5. Conclusion

Using computational homogenization and topology optimization, a design method for variable density and multi-lattice structures with high stiffness, light weight, and equivalent elastic properties of various strut-based lattice structures with small edge fillet are presented. The relationship between the relative strut diameter and relative density for six types of lattice structures is expressed as a fifth-order regression equation to determine the geometric dimensions of the lattice structure in terms of the relative density. At a relative density of 0.3, the SC_R lattice strut diameter of 0.41 is about 2.43 times larger than that of the OTC_R of 0.169. At the same relative density, several differences are observed in the diameter of the struts depending on the type of the lattice structure. The equivalent elastic properties of the lattice structure unit cell with edge fillet corresponding to various relative densities were obtained. The relationship between the equivalent elastic properties and relative density was expressed as a fourth-order regression equation. At a relative density of 0.3, the elastic modulus of the BCC_R lattice structures and shear modulus of the OTC_R lattice structures with edge fillets increased by greater than or equal to 18.5 % and 8.7 %, respectively, when compared with those of the model without edge fillets. The small edge fillet of the lattice structure contributed to the increased equivalent elastic properties and improved the anisotropy of the lattice under equal-weight conditions.

Compression simulations of a six-layered lattice are performed on the full-shape and homogenized lattice structure models to validate the predicted equivalent elastic properties. As a result, an initial stiffness difference of approximately 3 % is observed between the two models. For the lightweight and high stiffness design of lattice-based sandwich panels, topology optimization is performed to identify an optimized relative density distribution that satisfies the minimum compliance in the core. Variable-density lattice-based sandwich panels are designed using optimal relative density distribution obtained from the topology optimization. Three-point bending simulations are performed on approximately 14 types of sandwich panels with variable density distribution and lattice core using a homogenized lattice structure model to observe the mechanical properties according to the lattice types with small edge fillet, lattice combination, and relative density distribution. The variable-density and multi-lattice core sandwich panel models exhibited approximately 86.9 % higher initial stiffness than those with the conventional BCC uniform density cores. The optimized design method that considered the variable density, multi-lattice, equivalent elastic properties, fillet edge effect, and orientation of the lattice is a very useful method to increase the lightness in weight and stiffness of the lattice structure.

Because the computation time and high-performance systems have limitations, the homogenized lattice models will be useful in evaluating the mechanical properties of complex lattice models using computational simulation.

Acknowledgments

This work was supported by the National Research Foundation of Korea (NRF) grant funded by the Korean government (MSIT) (No. 2019R1A5A808320112), and also, it was partially supported by the “Human Resources Program in Energy Technology” of Energy Technology Evaluation and Planning (KETEP) in Korea (No. 20184010201660), and KETEP project (No. 20173030041340).

References

[1] D. Herzog, V. Seyda, E. Wycisk and C. Emmelmann, Additive manufacturing of metals, *Acta Materialia*, 117 (2016) 371-392.

[2] Y. Zhai, D. A. Lados and J. L. LaGoy, Additive manufacturing: making imagination the major limitation, *JOM*, 66 (5) (2014) 808-816.

[3] S. A. M. Tofail, E. P. Koumoulos, A. Bandyopadhyay, S. Bose, L. O’Donoghue and C. Charitidis, Additive manufacturing: scientific and technological challenges, market update and opportunities, *Materials Today*, 21 (1) (2018) 22-37.

[4] C. K. Chua and K. F. Leong, *3D Printing and Additive Manufacturing: Principles and Applications, Fifth Edition of Rapid Prototyping*, World Scientific Publishing Company: Singapore (2016).

[5] L. Zhu, N. Li and P. R. N. Childs, Light-weighting in aerospace component and system design, *Propulsion and Power Research*, 7 (2) (2018) 103-119.

[6] K. N. Son, J. A. Weibel, V. Kumaresan and S. V. Garimella, Design of multifunctional lattice-frame materials for compact heat exchangers, *International Journal of Heat and Mass Transfer*, 115 (2017) 619-629.

[7] R. Liu, Z. Wang, T. Sparks, F. Liou and J. Newkirk, 13-Aerospace applications of laser additive manufacturing, *Laser Additive Manufacturing*, (2017) 351-371.

[8] J. H. Yu, K. Y. Lee, D. -S. Shim and S. -H. Park, Metal embedding and ultrasonic nanocrystal surface modification technology for super wear-resistant mechanical parts, *International Journal of Advanced Manufacturing Technology*, 101 (2019)

951-962.
[9] C. Yang, M. Boorugu, A. Dopp, J. Ren, R. Martin, D. Han, W. Choi and H. Lee, 4D printing reconfigurable, deployable and mechanically tunable metamaterials, *Materials Horizons*, 6 (2019) 1244-1250.
[10] Y. Y. C. Choong, S. Maleksaeedi, H. Eng, S. Yu, J. Wei and P. C. Su, High speed 4D printing of shape memory polymers with nanosilica, *Applied Material Today*, 18 (2020) 100515.
[11] B. G. Compton and J. A. Lewis, 3D-printing of lightweight cellular composites, *Advanced Materials*, 26 (34) (2014) 5930-5935.
[12] H. Eng, S. Maleksaeedi, S. Yu, Y. Y. C. Choong, F. E. Wiria, R. E. Kheng, J. Wei, P. C. Su and H. P. Tham, Development of CNTs-filled photopolymer for projection stereolithography, *Rapid Prototyping Journal*, 23 (1) (2017) 129-136.
[13] Y. Y. C. Choong, H. W. Tan, D. C. Patel, W. T. N. Choong, C. H. Chen, H. Y. Low, M. J. Tan, C. D. Patel and C. K. Chua, The global rise of 3D printing during the COVID-19 pandemic, *Nature Reviews Materials*, 5 (2020) 637-639.
[14] M. Abdi, I. Ashcroft and R. D. Wildman, Design optimisation for an additively manufactured automotive component, *International Journal of Powertrains*, 7 (2018) 142-161.
[15] G. D. Goha, S. Agarwalaa, G. L. Goha, V. Dikshitb, S. L. Singa and W. Y. Yeong, Additive manufacturing in unmanned aerial vehicles (UAVs): challenges and potential, *Aerospace Science and Technology*, 63 (2017) 140-151.
[16] L. Zhang, S. Feih, S. Daynes, S. Chang, M. Y. Wang, J. Wei and W. F. Lu, Energy absorption characteristics of metallic triply periodic minimal surface sheet structures under compressive loading, *Additive Manufacturing*, 23 (2018) 505-515.
[17] A. G. Evans, J. W. Hutchinson and M. F. Ashby, Multifunctionality of cellular metal systems, *Progress in Materials Science*, 43 (1999) 171-221.
[18] F. Rissa, J. Schilpa and G. Reinhart, Load-dependent optimization of honeycombs for sandwich components-new possibilities by using additive layer manufacturing, *Physics Procedia*, 56 (2014) 327-335.
[19] L. Yang, O. Harrysson, H. West and D. Cormier, A comparison of bending properties for cellular core sandwich panels, *Materials Sciences and Applications*, 4 (8) (2013) 471-477.
[20] X. Zhang, H. Zhou, W. Shi, F. Zeng, H. Zeng and G. Chen, Vibration tests of 3D printed satellite structure made of lattice sandwich panels, *AIAA Journal*, 56 (10) (2018) 4213-4217.
[21] K. J. Maloney, K. D. Fink, T. A. Schaedler, J. A. Kolodziejska, A. J. Jacobsen and C. S. Roper, Multifunctional heat exchangers derived from three-dimensional micro-lattice structures, *International Journal Heat Mass Transfer*, 55 (2012) 2486-2493.
[22] T. J. Lu, L. Valdevit and A. G. Evans, Active cooling by metallic sandwich structures with periodic cores, *Progress in Materials Science*, 50 (2005) 789-815.
[23] W. Gao, Y. Zhang, D. Ramanujan, K. Ramani, Y. Chen, C. B. Williams, C. C. L. Wang, Y. C. Shin, S. Zhang and P. D. Zavattieri, The status, challenges, and future of additive manufacturing in engineering, *Computer-Aided Design*, 69 (2015) 65-89.
[24] M. K. Thompson, G. Moroni, T. Vaneker, G. Fadel, R. I. Campbell, I. Gibson, A. Bernard, J. Schulz, P. Graf, B. Ahuja and F. Martina, Design for additive manufacturing: trends, opportunities, considerations, and constraints, *CIRP Annals – Manufacturing Technology*, 65 (2016) 737-760.
[25] D. Mahmoud and M. A. Elbestawi, Lattice structures and functionally graded materials applications in additive manufacturing of orthopedic implants: a review, *Journal of Manufacturing and Materials Processing*, 1 (2) (2017) 13-31.
[26] E. Alabort, D. Barba and R. C. Reed, Design of metallic bone by additive manufacturing, *Scripta Materialia*, 164 (2019) 110-114.
[27] I. Maskery, A. O. Aremu, L. Parry, R. D. Wildman, C. J. Tuck and I. A. Ashcroft, Effective design and simulation of surface-based lattice structures featuring volume fraction and cell type grading, *Materials and Design*, 155 (2018) 220-232.
[28] P. Chopra, Effective mechanical properties of lattice materials, *M.A. Sc. Dissertation*, University of British Columbia, Vancouver, Canada (2011).
[29] M. -S. Pham, C. Liu, I. Todd and J. Lertthanasarn, Damage-tolerant architectured materials inspired by crystal microstructure, *Nature*, 565 (2019) 305-311.
[30] V. S. Deshpande, N. A. Fleck and M. F. Ashby, Effective properties of the octet-truss lattice material, *Journal of the Mechanics and Physics of Solids*, 49 (8) (2001) 1747-1769.
[31] G. D. Pasquale, M. Montemurro, A. Catapano, G. Bertolino and L. Revelli, Cellular structures from additive processes: design, homogenization and experimental validation, *Procedia Structural Integrity*, 8 (2018) 75-82.
[32] S. Xu, J. Shen, S. Zhou, X. Huang and Y. M. Xie, Design of lattice structures with controlled anisotropy, *Materials and Design*, 93 (2016) 443-447.
[33] L. Yang, C. Yan, H. Fan, Z. Li, C. Cai, P. Chen, Y. Shi and S. Yang, Investigation on the orientation dependence of elastic response in Gyroid cellular structures, *Journal of the Mechanical Behavior of Biomedical Materials*, 90 (2019) 73-85.
[34] D. H. Chen and L. Yang, Analysis of equivalent elastic modulus of asymmetrical honeycomb, *Composite Structures*, 93 (2) (2011) 767-773.
[35] S. Arabnejad and D. Pasini, Mechanical properties of lattice materials via asymptotic homogenization and comparison with alternative homogenization methods, *International Journal of Mechanical Sciences*, 77 (2013) 249-262.
[36] A. Iltchev, V. Marcadon, S. Kruch and S. Forest, Computational homogenisation of periodic cellular materials: application to structural modelling, *International Journal of Mechanical Sciences*, 93 (2015) 240-255.
[37] L. J. Gibson and M. F. Ashby, *Cellular Solids: Structure and Properties*, Cambridge University Press, Cambridge (1997).
[38] M. Kaur, T. G. Yun, S. M. Han, E. L. Thomas and W. S. Kim, 3D printed stretching-dominated micro-trusses, *Materials and Design*, 134 (2017) 272-280.
[39] A. Panesar, M. Abdi, D. Hickman and I. Ashcroft, Strategies for functionally graded lattice structures derived using topology optimisation for Additive Manufacturing, *Additive Manufacturing*, 19 (2018) 81-94.

[40] M. Alzahrani, S. K. Choi and D. W. Rosen, Design of truss-like cellular structures using relative density mapping method, *Materials and Design*, 85 (2015) 349-360.
[41] L. Cheng, P. Zhang, E. Biyikli, J. Bai, J. Robbins and A. To, Efficient design optimization of variable-density cellular structures for additive manufacturing: theory and experimental validation, *Rapid Prototyping Journal*, 23 (4) (2017) 660-677.
[42] D. Li, W. Liao, N. Dai, G. Dong, Y. Tang and Y. M. Xe, Optimal design and modeling of gyroid-based functionally graded cellular structures for additive manufacturing, *Computer-Aided Design*, 104 (2018) 87-99.
[43] M. F. Ashby and Y. J. M. Brechet, Designing hybrid materials, *Acta Materialia*, 51 (2003) 5801.
[44] L. R. Meza, G. P. Phlipot, C. M. Portela, A. Maggi, L. C. Montemayor, A. Comella, D. M. Kochmann and J. R. Greer, Reexamining the mechanical property space of three-dimensional lattice architectures, *Acta Materialia*, 140 (2017) 424.
[45] L. Cheng, J. Bai and A. C. To, Functionally graded lattice structure topology optimization for the design of additive manufactured components with stress constraints, *Computer Methods in applied Mechanics and Engineering*, 344 (2019) 334-359.
[46] D. S. Kang, S. H. Park, Y. Son, S. M. Yeon, S. H. Kim and I. Y. Kim, Multi-lattice inner structures for high-strength and lightweight in metal selective laser melting process, *Materials and Design* (2019) 175107786.
[47] J. Plocher and A. Panesar, Review on design and structural optimisation in additive manufacturing: towards next-generation lightweight structures, *Materials and Design*, 183 (2019) 108164.
[48] S. Daynes, S. Feih, W. F. Lu and J. Wei, Optimisation of functionally graded lattice structures using isostatic lines, *Materials and Design*, 127 (2017) 215-223.
[49] L. Huynh, J. Rotella and M. D. Sangid, Fatigue behavior of IN718 microtrusses produced via additive manufacturing, *Materials and Design*, 105 (2016) 278-289.
[50] T. Maconachie, M. Leary, B. Lozanovski, X. Zhang, M. Qian, O. Faruque and M. Brandt, SLM lattice structures: properties, performance, applications and challenges, *Materials and Design*, 183 (2019) 108137.
[51] J. R. C. Dizon, A. H. Espera Jr., Q. Chena and R. C. Advincula, Mechanical characterization of 3D-printed polymers, *Additive Manufacturing*, 20 (2018) 44.
[52] D. Kazmer and M. Kutz (Ed.), Three-dimensional printing of plastics, applied plastics engineering handbook-processing, materials, and applications, *A Volume in Plastics Design Library,* 2nd Edition (2017).
[53] K.-W. Lee, S.-H. Lee, K.-H. Noh, J.-Y. Park, Y.-J. Cho and S.-H. Kim, Theoretical and numerical analysis of the mechanical responses of BCC and FCC lattice structures, *Journal of Mechanical Science and Technology*, 33 (2019) 2259.

Ho Seung Jeong is a Research Professor in the School of Mechanical Engineering at Pusan National University. He earned his M.S. and Ph.D. in Mechanical Engineering at Korea Maritime and Ocean University in 2001 and 2005, respectively. His research fields are the engineering for additive manufacturing, metal forming, thermo-mechanical analysis, and optimal design.

Sung Ki Lyu is a Professor in the School of Mechanical & Aerospace Engineering of Gyeongsang National University. He earned his M.S. in Mechanical Engineering at Jeonbuk National University in 1989 and his Ph.D. in Precision Engineering at Tohoku University, Japan in 1994. His research fields are gear, gearbox, mechanical system design, control mechanics, power transmission system, fatigue and strength evaluation, and so on.

Sang Hu Park is a Professor in the School of Mechanical Engineering at Pusan National University. He earned his M.S. and Ph.D. in Mechanical Engineering at Korea Advanced Institute of Science and Technology (KAIST) in 1996 and 2006, respectively. His research fields are the engineering for additive manufacturing, sheet metal forming, and nanofabrication.